A Frequency Diversity Pulse-Pair Algorithm for Extending Doppler Radar Velocity Nyquist Range

V. Venkatesh
Science Systems and Applications Inc.
and NASA Goddard Space Flight center
Greenbelt, MD, USA
Email: vijay.venkatesh@nasa.gov

L. Li
M. McLinden
G. Heymsfield
M. Coon
NASA Goddard Space Flight Center
Greenbelt, MD, USA

***Abstract*—Millimeter wave radars have been widely used for atmospheric remote sensing and tracking hard-targets from airborne platforms. For these radars, the product of the unambiguous range and Doppler velocity is limited by the radar wavelength. This work focuses on a novel method to extend the Nyquist rate of millemeter radars, which uses frequency diversity pulse-pairs for Doppler phase estimation. Two short pulses with center-frequencies of f_1 followed by f_2 are transmitted during the first pulse repetition interval (PRI). During the next PRI, the pulses transmitted are in the order f_2 followed by f_1 respectively. There are two mechanisms for error reduction. First, the "beat" phases of the f_1/f_2 and f_2/f_1 pairs cancel out in the expected value sense. Second, since the f_1/f_2 and f_2/f_1 phase estimates are highly anti-correlated, the sum of the two phase estimates has a much smaller variance than the individual phase estimates. Based on Monte-Carlo simulations, the feasibility of this method is demonstrated herein. Ongoing data analysis is discussed.**

I. Introduction

Millimeter wave radars have been widely used for atmospheric remote sensing and tracking hard-targets from airborne platforms [1-5]. In large part, the popularity of these millimeter wave radars is because fine antenna beamwidths can be realized while still allowing for physically small and lightweight designs, as well as higher backscattering efficiency for weather targets such as cloud particles. However, the product of the unambiguous range and Doppler velocity is limited by the radar wavelength (i.e. $\frac{c\lambda}{8}$)). Airborne millimeter wave radars that are required to have long range coverage therefore may have Doppler Nyquist ranges that are much smaller than the relative speeds of competing aircrafts.

Different techniques to mitigate the Doppler-Range ambiguity dilemma have been explored. For example, the staggered PRT [6] and Polarization Diverse Pulse-Pair (PDPP) [7] techniques are methods that are already employed for these purposes. The "staggered" PRT is a multi-rate sampling method that unfolds the Doppler velocity based on the ratio of Doppler velocities measured by 2 PRTs. A weakness of this approach is that the resulting Doppler velocity estimates have increased sensitivity to noise, relative to the usage of a single PRT. The Polarization Diversty Pulse-Pair method utilizes two pulses with orthogoal polarizations. These two pulses can be placed with shorter time interval to extend the Doppler Nyquist range, while the PRT can be adjusted independently for range coverage. Notwithstanding, finite polarization isolation of the antenna and the receivers may overwhelm retrievals close to regions with high SNR [7].

This work focuses on a novel alternative - which uses frequency diversity (in lieu of polarization diversity) pulse-pair for Doppler phase estimation. Along with the cutting-edge digital waveform generation and digital receiver/processor technologies, this frequency diversity pulse-pair technique can be easily implemented on a modern radar without additional microwave hardware. If proven practical, this frequency diverse pulse-pair method would potentially enable low-cost and light weight air-borne millimeter wave radars with wide Nyquist Doppler capability. The following section outlines the theoretical formulation of the Frequency Diversity Pulse-Pair algorithm (FDPP). Numerical simulations are then presented to validate the theory developed herein.

II. Methodology

A. Conceptual description of FDPP algorithm

Two pulses at center frequencies of f_1 and f_2 are transmitted with a separation of lag ΔT. While retaining ΔT, the order of the pulses is reversed every alternate transmission. From the receive channels at f_1 and f_2, the pulse-pair phase estimate of the two sequences are individually accumulated and stored as $\Delta\phi_{order1}$ and $\Delta\phi_{order2}$. Finally Doppler velocity is estimated from the sum of an equal number of the two individual pulse-pair phase estimates (denote as $\Delta\phi$). Note that the use of two closely spaced radar frequencies introduces two primary sources of error. First, a "beat" phase that scales as a function of range is introduced. Nonetheless, this term vanishes when the phases of the f_1/f_2 pair and f_2/f_1 pairs are added.Second, since there is little correlation between the f_1 and f_2 pulses, the variances of the f_1/f_2 phase estimates is large. However, since the f_1/f_2 and f_2/f_1 phase estimates are highly anti-correlated, the sum of the two phase estimates has a much smaller variance.

B. Mathematical description of FDPP algorithm

Denote the transmitted waveform at frequency f_1 as $E_{Tx,f1}(t)$. Let $E_{0,f1}$ be the amplitude of the transmitted signal, the phase of the transmitted signal be $\Psi_{Tx,f1}$ and t denote time.

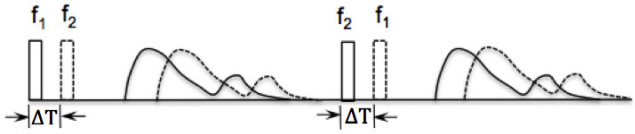

Fig. 1. Illustration of the Frequency Diversity Pulse-Pair (FDPP) concept. Two short pulses with center-frequencies of f_1 and f_2 are transmitted during the first pulse repetition interval (PRI). During the next PRI, the pulses are transmitted in the order of f_2 and f_1 respectively. There are two mechanisms for error cancellation. First, the "beat" phases of the f_1-f_2 and f_2-f_1 pairs cancel out in the expected value sense. Second, since the f_1-f_2 and f_2-f_1 phase estimates are highly anti-correlated, the sum of the two phase estimates has a much smaller variance than the individual phase estimates.

$$E_{Tx,f1}(t) = E_{0,f1}cos[2\pi f_1 t + \Psi_{Tx,f1}] \quad (1)$$

Denote c be the speed of light, f_{D1} be the Doppler shift and R the range to a point scatterer. Now, the received signal $E_{Rx,f1}$ at time t can be written as

$$E_{Rx,f1}(t) = A_{f1}E_{0,f1}cos[2\pi(f_1 + f_{D1})(t + \frac{2R}{c}) + \Psi_{Tx,f1}] \quad (2)$$

Similarly, the Tx and Rx signals at frequency f_2 and time $t + \Delta T$ can be written as follows. Note that the range to the point-scatterer is now $R + v_r\Delta T$. Here, v_r denotes the radial velocity of the point-scatterer.

$$E_{Tx,f2}(t + \Delta T) = E_{0,f2}cos[2\pi f_2(t + \Delta T) + \Psi_{Tx,f2}] \quad (3)$$

$$E_{Rx,f2}(t + \Delta T) = A_{f2}E_{0,f2}cos[2\pi(f_2 + f_{D2})(t + \tfrac{2R+v_r\Delta T}{c}) + \Psi_{Tx,f2}]$$

Assume $A_{f1} = A_{f2}$, $E_{0,f1} = E_{0,f2}$, $f_1 \gg f_{D1}$ and $f_2 \gg f_{D2}$. Denote the echo phase $\phi_{Rx} - \phi_{Tx}$ for the frequencies f_1 and f_2 as Φ_{f1} and Φ_{f2} respectively.

$$\Phi_{f1} = 2\pi f_1(t + \frac{2R}{c}) + \Psi_{Tx,f1} - 2\pi f_1 t - \Psi_{Tx,f1} \quad (4)$$

$$\Phi_{f1} = 2\pi f_1 \frac{2R}{c} \quad (5)$$

$$\Phi_{f2} = 2\pi f_2[(t + \Delta T) + \frac{2(R + \Delta T)}{c}] - 2\pi f_2(t + \Delta T) \quad (6)$$

$$\Phi_{f2} = 2\pi f_2 \frac{2R + 2v_r\Delta T}{c} \quad (7)$$

The frequency-diversity pulse pair algorithm is based on the two qauntities $\Delta\Phi_{order1}$ and $\Delta\Phi_{order2}$. Here, $\Delta\Phi_{order1} = \Phi_{f2} - \Phi_{f1}$ and $\Delta\Phi_{order2} = \Phi_{f1} - \Phi_{f2}$. Denote $\lambda_1 = c/f_1$, $k_1 = \frac{2\pi}{\lambda_1}$, $\lambda_2 = c/f_2$ and $k_2 = \frac{2\pi}{\lambda_2}$.

$$\Delta\Phi_{order1} = 2R_{order1}(k_1 - k_2) + 2k_1 v\Delta T \quad (8)$$

Similarly,

$$\Delta\Phi_{order2} = 2R_{order2}(k_2 - k_1) + 2k_2 v\Delta T \quad (9)$$

Recognizing that $R_{order2} = R_{order1} + v\tau$. Here τ denotes the pulse repetition time. Denote $\Delta\Phi = \Delta\Phi_{order1} + \Delta\Phi_{order2}$.

$$\Delta\Phi = 2(k_2 - k_1)v_r\tau + 2(k_1 + k_2)v_r\Delta T \quad (10)$$

$$\Delta\Phi = 2[(k_2 - k_1)\tau + (k_1 + k_2)\Delta T]v_r \quad (11)$$

The implementation we consider herein typically has frequencies that are spead apart by a few MHz. Therefore, the term $k_2 - k_1$ can be neglected in the context of the rest of the equation. Further, we approximate $k_1 + k_2 \approx 2k_1$. The above equation simplifies to the following -

$$v_r = \frac{1}{4k_1\Delta T}\Delta\Phi \quad (12)$$

Since all values other than $\Delta\Phi$ are solely system dependent, the radial component of target mean radial velocity v_r can be obtained from the ensemble-averaged $\Delta\Phi$. Two comments about the Nyquist velocity of the frequency diversity pulse-pair equation are in order. First, for a given lag ΔT the Nyquist interval is diminished by a factor of 2 compared to a traditional pulse-pair or a polarization diversity pulse-pair. This is because the frequency diversity pulse-pair algorithm accumulates two phase estimates $\Delta\Phi_{order1}$ and $\Delta\Phi_{order2}$ and the resultant sum has a range of variation from $[-\pi, \pi]$. Second, the frequency diversity pulse-pair algorithm developed herein allows an extension of the Nyquist interval as compared to a traditional pulse-pair which necessarily needs long lags to accomodate sufficiently unambiguos ranges. For example, if the FDPP algorithm is denoted by lag ΔT and the pulse-pair algorithm denoted by a lag τ, then the Nyquist interval of the FDPP algorithm is improved by a factor $\frac{\tau}{2\Delta T}$.

A short analysis of the error of the FDPP phase estimate is in order. To this end, let σ denote the variance and ρ denote the correlation operators respectively.

$$\sigma(\Delta\Phi) = \sigma(\Delta\Phi_{Order1}) + \sigma(\Delta\Phi_{Order2}) + 2Cov(\Delta\Phi_{order1}, \Delta\Phi_{order2})$$

Now, the covariance term can be conveniently decomposed as

$$Cov(\Delta\Phi_{Order1}, \Delta\Phi_{Order2}) = \rho(\Delta\Phi_{Order1}, \Delta\Phi_{Order2}) \cdot \sqrt{\sigma(\Delta\Phi_{Order1}) \cdot \sigma(\Delta\Phi_{Order2})}$$

For cases where $\sigma(\Delta\Phi_{Order1}) = \sigma(\Delta\Phi_{Order2})$,

$$Cov(\Delta\Phi_{Order1}, \Delta\Phi_{Order2}) = \rho(\Delta\Phi_{order1}, \Delta\Phi_{order2}) \cdot \sigma(\Delta\Phi_{Order1})$$

From the above relationships,

$$\sigma(\Delta\Phi) = 2\sigma(\Delta\Phi_{Order1}) + 2\rho(\Delta\Phi_{Order1}, \Delta\Phi_{Order2}) \cdot \sigma(\Delta\Phi_{Order1}) \quad (13)$$

Rearranging terms in (13),

$$\sigma(\Delta\Phi) = 2\sigma(\Delta\Phi_{Order1})[1+\rho(\Delta\Phi_{Order1}, \Delta\Phi_{Order2})] \quad (14)$$

The underlying premise of the frequency-diversity pulse-pair algorithm is that as $\rho(\Delta\Phi_{Order1}, \Delta\Phi_{Order2}) \rightarrow -1$, the variance of the phase composite estimate $\sigma(\Delta\Phi) \rightarrow 0$.

C. Simulation methodology

Our approach to numerical simulations is to estimate the phases at lag ΔT using simulated backscattered electric fields at the antenna port using a Monte-Carlo based simulator. Specifically, the voltage due to backscattered electric fields at the receiver is given as

$$V(t) = A \cdot R \cdot T \exp\{-2jkr_0\}. \quad (15)$$

Here, T the backscattering amplitude due to scattering from a Swerling III-type target, A denotes the antenna weighting function and R the range weighting function. The amplitude fluctations T of the target are samples from a fourth order Chi-squared distribution as illustrated in Figure 1. Here the black line shows power fluctuations due to a Swerling type III target. The red curve - with the x and y-axes indicated in red - shows the probability density function for the backscattering efficiency. In essence, this is the PDF for voltage at the receiver as the change in antenna and range weighting functions is small over the period of the dwell considered herein. The antenna weighting function is defined below

$$A = \exp\left\{-\frac{(X_0 - X)^2}{2r_0^2\sigma_\phi^2} - \frac{(Y_0 - Y)^2}{2r_0^2\sigma_\theta^2}\right\} \quad (16)$$

where the antenna phase center is denoted by $[X_0, Y_0]$, the hard-target location is indicated by $[X, Y]$ and σ_ϕ and σ_θ are the second central moment of the effective two way antenna patterns in the azimuthal and elevational planes respectively. The range weighting function and its relationship to transmitted chirp bandwidth is given by

$$R_n = \exp\left\{-\frac{(Z_0 - Z)^2}{2\sigma_R^2}\right\} \quad (17)$$

$$\sigma_R = 0.35\frac{c}{2B} \quad (18)$$

where, Z_0 is the center of the resolution volution in range, Z indicates the scatterer location, c is the speed of light (m/s) and B is the transmitted chirp bandwidth. The constant 0.35 approximately accounts for losses due to amplitude modulation of the chirp and finite receiver bandwidth.

Scatterer locations are updated at every pulse repetition interval given mean and relatively small fluctating velocity components along each coordinate. Gaussian distributed pseudo-random values are used to generate the fluctuating velocity fields. Since the omission of temporal continuity of the fluctuating velocity causes the scatterer to have abrupt changes in position, we run a 5-point moving average filter to low-pass filter the fluctuating velocity in the temporal dimension. It is this low-pass filtering by the moving average filter that distinguishes velocity variations from random Brownian motion and from random changes in the phase of the composite signal introduced by thermal noise.

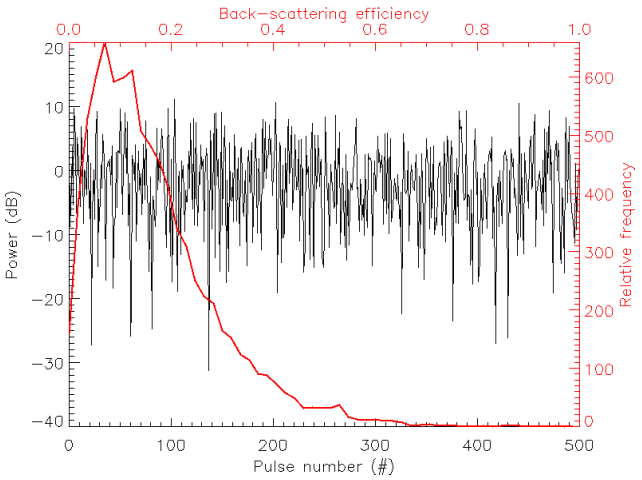

Fig. 2. Illustration of Swerling III type target amplitude fluctuations. The red line - with the corresponding axes indicated in red -shows fluctuations in backscattering efficiency. In practice, this corresponds to voltage fluctuations as the variation of the antenna and range weighting functions are negligible over the period of the dwell. The black line - with the corresponding axes in black - shows the fluctuations in power of the synthesized time-series.

Once the time series data is generated , thermal noise is added . Phase estimates at the lag ΔT are then obtained for the sequences f_1/f_2 and f_2/f_1. Typically, 1000 trials are performed in order to produce the statistics of the next section.

III. Preliminary Results

In this section, Monte-Carlo simulations are qualitatively compared with data-analysis results (all at W-band). Fig. 3 shows simulations of the FDPP Doppler velocity retrieval process. The basic idea is that a composite phase that is solely Doppler dependent is synthesized from noisy but highly anti-correlated frequency diverse pulse-pair lag-1 phase estimates. The phase estimate from the sequence in which f_1 leads f_2 is shown in Fig. 3a. After 1 PRT, the sequence of f_2 followed by f_1 is yields phase estimates shown in Fig. 3b. The sum of the two frequency diverse pulse-pair estimates is shown in Fig. 3c. Fig. 3d shows a scaled version of Fig.3c, where the composite phase is scaled to the Doppler Nyquist interval.

Fig. 4 shows the FDPP algorithm Doppler retrieval accuracy for a W-band radar as a function of various design parameters. The simulation methodology employed herein is similar to that in [7]. Typically, 1000 Monte-Carlo tries were employed to generate the simulation statistics. The relevant parameters shown in the corresponding figures. In Fig. 4a, the increasing errors on the right side are a direct consequence of decreasing correlation between the f_1/f_2 and f_1/f_2 pair phase estimates. The increasing errors on the left hand side are due to sensitivity to thermal noise. As expected, this is exacerbated at shorter lags and decreasing SNR. Similar reasoning deems a 3 kHz pulse repetition frequency (PRF) optimal in Fig. 4b. In Fig. 4c,

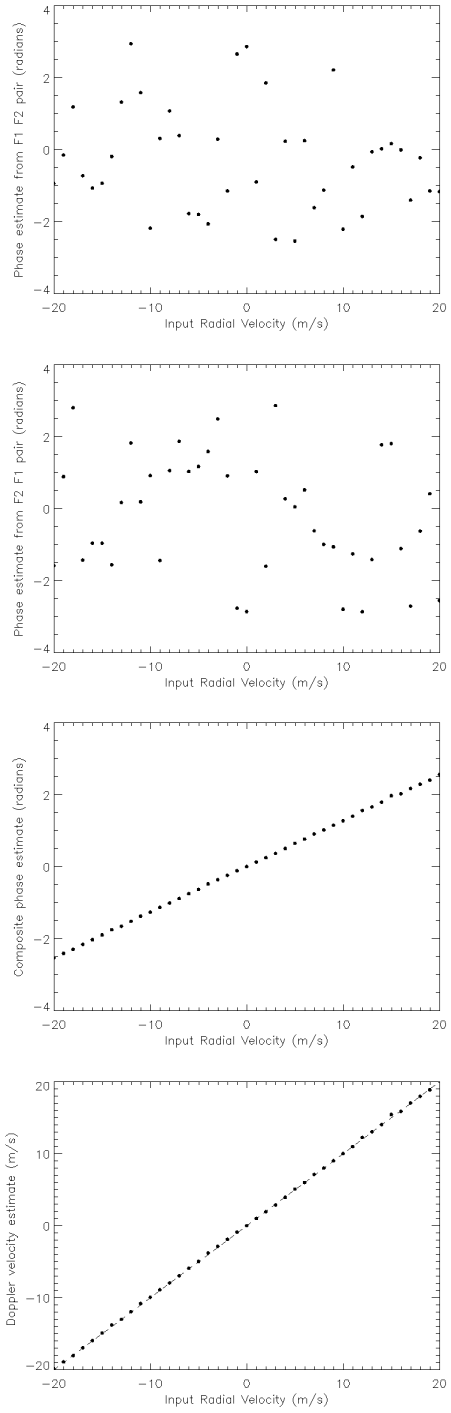

Fig. 3. Monte-Carlo simulations showing the FDPP algorithm concept. Clockwise from top left. (a) Phase estimates from f_1-f_2 pulse-pair ($\Delta\phi_{order1}$). (b) Phase estimates from f_2-f_1 pulse-pair ($\Delta\phi_{order2}$). (c) Sum of Fig. 2a and 2b., after unwrapping. (d) FDPP Doppler estimates using a scaled version of (c).

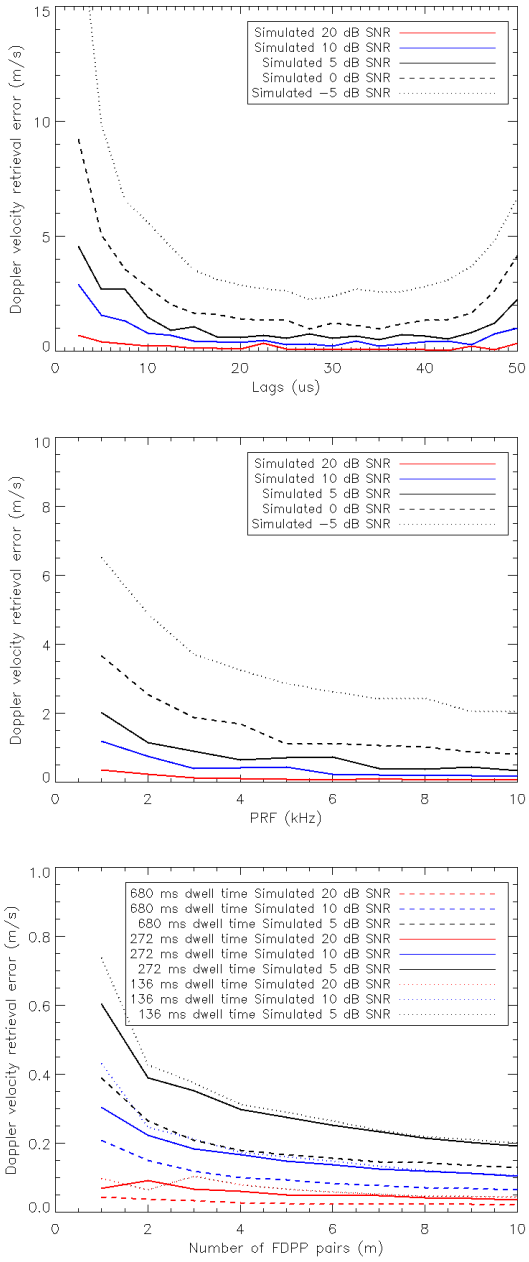

Fig. 4. Monte-Carlo simulations of the FDPP algorithm error space. (a) FDPP Doppler retrieval error as a function of time-lag. (b) FDPP Doppler retrieval error as a function of Pulse Repetition Frequency. (c) FDPP Doppler retrieval accuracy as a function of number of simultaneously transmitted/received FDPP pairs for 136 millisecond, 272 millisecond and 680 milliseconds dwell times.

the increasing errors on the right side are a direct consequence of decreasing correlation between the f_1/f_2 and f_1/f_2 pair phase estimates. The increasing errors on the left hand side are due to sensitivity to thermal noise.

Fig. 5 shows preliminary data analysis results using NASA's Cloud Radar System (CRS) during the OLYMPEX mission. The CLoud Radar System was mounted on an ER-2 aircraft with the antenna pointed "nearly" at nadir. Aircraft attitude fluctuations cause the antenna to point slightly away from nadir, thereby inducing a surface velocity measurement contaminated with the motion of the aircraft. Traditional pulse-pair measurements are used as "truth" and compared to the frequency diversity algorithm developed herein. Two comments are in order. First, high SNR cases from the surface were isolated for this analysis to be consistent with the simulation predictions that the algorithm requires high SNR to yield reasonable estimates. For most part, we also expect that they have lower spectrum width as compared to the layer of clouds evident in the Fig. 5a. Second, Fig. 5b shows excellent agreement of the frequency diverse pulse-pair algorithm with traditional pulse-pair measurements. In essence, this validates the approach developed herein to first order. More detailed analysis of the error space is ongoing at NASA Goddard Space Flight Center.

IV. Summary

Herein, we have investigated a novel algorithm to overcome the Doppler-Range velocity dilemma using millimeter wave radars. The frequency diversity pulse-pair algorithm first transmits a sequence of two pulses modulated by frequencies f_1 and f_2 in that order. During the next sequence the order of f_2 and f_1 are reversed. In both cases, the pulses are seperated by a time lag ΔT. The sum of the phase estimates from the f_1/f_2 and f_2/f_1 pairs yields a resultant phase which is linearly related to Doppler velocity. There are two mechanisms for error reduction. First, the "beat" phases of the f_1/f_2 and f_2/f_1 pairs cancel out in the expected value sense. Second, since the f_1/f_2 and f_2/f_1 phase estimates are highly anti-correlated, the sum of the two phase estimates has a much smaller variance than the individual phase estimates. The error space of the algorithm was investigated with Monte-Carlo simulations.Based on numerical simulations, the algorithm was deemed to require high SNR. Data was collected using NASA's Cloud Radar System and the high SNR data points from the surface showed excellent agreement with traditional pulse pair-estimates of Doppler velocity. More detailed analysis is ongoing at Goddard.

With modern digital waveform generation, digital receiver and solid-state power amplifier technologies, FDPP can be implemented without additional microwave hardware like a second receiver channel. Compared to PDPP, FDPP provides better channel isolation, therefore better mitigates contamination from strong targets. Monte-Carlo simulations and preliminary data analysis indicate that the algorithm has strong potential for applications such as correcting space-borne radar

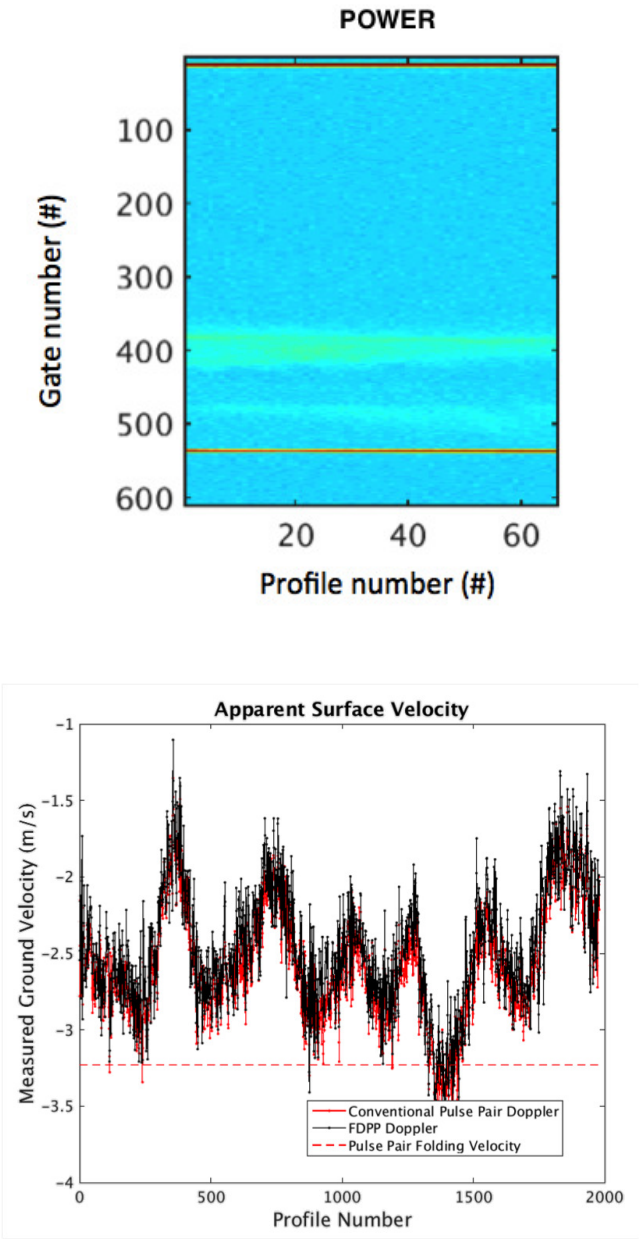

Fig. 5. Data analysis from NASA's Cloud Radar System during the OLYMPEX mission. (a) Power profiles collected during a segment of the flight on the ER-2 aircraft with the antenna pointing "nearly" at nadir. Changes in aircraft attitude cause the antenna to point away from nadir thereby measuring a surface velocity contaminated with the aircraft motion. Note that the surface has high received power, and a layer of clouds above the surface has much lower received power. (b) Quantivative comparisons of the frequency diversity pulse-pair algorithm estimates with traditional pulse-pair algorithm measurements. Note that the FDPP estimates track the changes in pulse-pair velocity measurements very well. More quantitative analysis is underway at NASA Goddard Spaceflight Center.

antenna pointing errors, air-traffic control. military aircraft and missile tracking.

REFERENCES

[1] Pazmany, A.L. and McIntosh and Kelly R., *An airborne 95 GHz dual polarization radar for cloud studies* IEEE Trans. Geosci. Remote Sensi., 32, No. 4, 731-739, 1994.

[2] L.Li and G. Heymsfield and P. Racette and L. Tian and E. Zenker, *A 94 GHz cloud radar system on a NASA high-altitude ER-2 aircraft*. J. Atmos. Oceanic. Tech., 21, 1378-1388, 2004.

[3] G.M. Brookner and D. Birch and J. Solms, *W-Band Airborne interrupted frequency modulated CW imaging radar.* IEEE Trans. on Aerosp. Electron. Syst., 41, No. 3, 995-972, 2005.

[4] Sajadi, F. and Helgeson and M. Radke and Steyn G., *Radar synthetic vision system for adverse weather aircraft landing.* IEEE Trans. on Aerosp. Electron. Syst., 35, No. 1, 2-14, 1999.

[5] Currie, N. and Brown, C., *Principles and Applications of millimeter-wave radar* Artech House, 1987.

[6] Sachidananda, M. and Zrnic, D.S., *Unambiguos range extension by overlay resolutin in staggered PRT technique.* J. Atmos. Oceanic. Tech., 20, 673-684, 2003.

[7] A. Pazmany and J. C. Galloway and J. Mead and I. Popstefanija and R. McIntosh and H. Bluestein, *Polarization diversity pulse-pair technique for millimeter wave doppler radar measurements of severe storm measurements*. J. Atmos. Oceanic. Tech., 16, 1900-1911, 1999.

[8] P. Amayenc and J. Testud and M. Marzoug, *Proposal for a spaceborne dual-beam rain radar with doppler capability*. J. Atmos. Oceanic. Tech., 10, 262-276, 1993.

[9] A. Battaglia and S. Tanelli, *Polarization diversity for millimeter wave spaceborne doppler radars: An answer for observing deep convection ?*. J. Atmos. Oceanic. Tech., 30, 2768-2787, 2013.

[10] W.-K. Tao and et al., *Retrieval of latent heating from TRMM measurements*, 3rd ed. Bull. Amer. Meteor. Soc., 87, 1555-1572.

[11] S. Koboyashi and H. Kumagai and H. Kuroiwa, *A proposal of pulse-pair doppler operation on a space-borne cloud profiling radar in the w-band*. J. Atmos. Oceanic. Tech., 19, 1294-1306, 2001.

[12] V. Venkatesh and S. J. Frasier, *Simulation of spaced antenna wind retrieval performance on an x-band active phased-array weather radar*. J. Atmos. Oceanic. Tech., 30, 1447-1459, 2013.

[13] D. Wilson and A. Illingworth and T. Blackman, *Differential doppler velocity: A radar parameter for charecterizing hydrometeor size distributions*. J. of App. Meteor., 36, 649-663, 1997.